

# Three-dimensional nonparaxial beams in parabolic rotational coordinates

Dongmei Deng,<sup>1,2</sup> Yuanmei Gao,<sup>2,3</sup> Juanying Zhao,<sup>2,4</sup> Peng Zhang,<sup>2,5</sup> and Zhigang Chen<sup>2,6,\*</sup>

<sup>1</sup>Laboratory of Nanophotonic Functional Materials and Devices, South China Normal University, Guangzhou 510631, China

<sup>2</sup>Department of Physics and Astronomy, San Francisco State University, San Francisco, California 94132, USA

<sup>3</sup>College of Physics and Electronics, Shandong Normal University, Jinan 250014, China

<sup>4</sup>School of Optoelectronics, Beijing Institute of Technology, Beijing 100081, China

<sup>5</sup>NSF Nanoscale Science and Engineering Center, University of California, Berkeley, California 94720, USA

<sup>6</sup>TEDA Applied Physics School, Nankai University, Tianjin 300457, China

\*Corresponding author: zhigang@sfsu.edu

Received May 9, 2013; revised August 27, 2013; accepted August 29, 2013;

posted September 3, 2013 (Doc. ID 190305); published September 30, 2013

We introduce a class of three-dimensional nonparaxial optical beams found in a parabolic rotational coordinate system. These beams, representing exact solutions of the nonparaxial Helmholtz equation, have inherent parabolic symmetries. Assisted with a computer-generated holography, we experimentally demonstrate the generation of different modes of these beams. The observed transverse beam patterns along the propagation direction agree well with those from our theoretical predication. © 2013 Optical Society of America

OCIS codes: (260.2110) Electromagnetic optics; (350.5500) Propagation; (070.3185) Invariant optical fields.

<http://dx.doi.org/10.1364/OL.38.003934>

Optical beams with subwavelength scales yet large bending angles are desirable for a variety of applications including near-field optical microscopes, plasmonics, and optical manipulation of nanoparticles [1–3]. Under the condition of large beam divergence or large beam bending, the conventional paraxial theory cannot fully describe the beam propagation. Therefore, free-space propagation of optical beams beyond the paraxial approximation continues to be a topic of great interest. To analyze nonparaxial optical beams, a few approaches have been developed: one is based on the high-order corrections to the known paraxial solution [4–6]; and the other relies on the so-called complex point source model [7]. In fact, nonparaxial beams should be described by wave equations without the paraxial approximation. In other words, such beams must be analyzed from the nonparaxial Helmholtz equation. Thus far, quite a few examples of nonparaxial beams have been obtained in different coordinate systems [8–13].

Motivated by the recent surge of interest in self-accelerating beams demonstrated from paraxial [14,15] to nonparaxial [16–20] regimes, we study in this Letter nonparaxial beams in parabolic rotational coordinates. We theoretically formulate and experimentally demonstrate such nonparaxial beams. Different from invariant propagation of nondiffracting Bessel beams, these beams exhibit the parabolic rotation symmetry during propagation, with their envelopes following along parabolic trajectories. Good agreement is found between experimental observation and our theoretical predication. We point out that although the exact solution of the Helmholtz equation in parabolic rotational coordinates has been studied for quantum mechanics and acoustics [21,22], the nonparaxial beams of parabolic rotational coordinates have never been introduced or demonstrated in optics. The propagation of nonparaxial optical beams in free space can be described by the following three-dimensional (3D) Helmholtz equation:

$$\frac{\partial^2 U}{\partial x^2} + \frac{\partial^2 U}{\partial y^2} + \frac{\partial^2 U}{\partial z^2} + k^2 U = 0, \quad (1)$$

where  $U(x, y, z)$  is the complex amplitude of the light field propagating along  $z$ ,  $k = k_0 n_0$ ,  $k_0 = 2\pi/\lambda$ , is the wave number in vacuum, and  $n_0$  is the refractive index of the medium. Introducing  $x = \xi\eta \cos \Phi$ ,  $y = \xi\eta \sin \Phi$ ,  $z_0 - z = (\xi^2 - \eta^2)/2$  [21,22] (where  $z_0$  is a positive constant),  $\xi \in (0, \infty)$ ,  $\eta \in (0, \infty)$ , and  $\Phi \in (0, 2\pi)$ , the parabolic rotational coordinates can be established. The constant  $\xi$  and  $\eta$  surfaces are both paraboloids with respect to the  $z$  axis, respectively. The parabolic rotational coordinate system is an orthogonal curvilinear one [21,22]. If we use the method of separation of variables, letting  $U(\xi, \eta, \Phi) = M(\xi)N(\eta)\Theta(\Phi)$ , where  $M$ ,  $N$ , and  $\Theta$  are complex functions, we obtain in the parabolic rotational coordinates system the following equations:

$$\frac{d^2 M(\xi)}{d\xi^2} + \frac{1}{\xi} \frac{dM(\xi)}{d\xi} + \left( -\frac{m^2}{\xi^2} + k^2 \xi^2 - \alpha k \right) M(\xi) = 0, \quad (2a)$$

$$\frac{d^2 N(\eta)}{d\eta^2} + \frac{1}{\eta} \frac{dN(\eta)}{d\eta} + \left( -\frac{m^2}{\eta^2} + k^2 \eta^2 + \alpha k \right) N(\eta) = 0, \quad (2b)$$

$$\frac{d^2 \Theta(\Phi)}{d\Phi^2} + m^2 \Theta(\Phi) = 0, \quad (2c)$$

where  $m$  and  $\alpha$  are the separation constants. Solutions of Eqs. (2a) and (2b) are given by hypergeometric functions [23]. Collecting the solutions of Eqs. (2a)–(2c), we construct the exact solution of the 3D Helmholtz as

$$\begin{aligned}
 U(\xi, \eta, \Phi) &= (\xi\eta/w_0)^m e^{\pm ik(\xi^2 + \eta^2)/2 + im\Phi} \\
 &\times {}_1F_1\left(\frac{i\alpha}{4} + \frac{m+1}{2}, m+1, \mp ik\xi^2\right) \\
 &\times {}_1F_1\left(-\frac{i\alpha}{4} + \frac{m+1}{2}, m+1, \mp ik\eta^2\right). \quad (3)
 \end{aligned}$$

From Eq. (3), the nonparaxial beams in parabolic rotational coordinates as exact solutions of Eq. (1) in the laboratory frame can be expressed as

$$\begin{aligned}
 U(x, y, z) &= (-1)^m [(x \pm iy)/w_0]^m e^{\pm ikr} \\
 &\times {}_1F_1\left(\frac{i\alpha}{4} + \frac{m+1}{2}, m+1, \mp ik(z_0 - z + r)\right) \\
 &\times {}_1F_1\left(-\frac{i\alpha}{4} + \frac{m+1}{2}, m+1, \mp ik(z - z_0 + r)\right), \quad (4)
 \end{aligned}$$

where  $w_0$  is a positive parameter with length dimension,  $r = \sqrt{x^2 + y^2 + (z_0 - z)^2}$ , and  $m$  corresponds to the azimuthal eigenvalue as referred to the topological charge for optical vortices. At  $i\alpha = 0$  and  $2(m+1)$ , Eq. (4) describes the Bessel wave [21,22] and the vortex plane wave. When  $i\alpha$  is an integer and  $i\alpha < -2(m+1)$ , Eq. (4) becomes the Laguerre wave [23]. When  $m = 0$ , Eq. (4) represents the fundamental solution of a nonparaxial parabolic rotational coordinate beam. We point out that the divergence angle of the beam is determined by the parameters in Eq. (4). Under paraxial approximation, namely  $r \approx z + (x^2 + y^2)/(2z)$ , Eq. (4) becomes the solution of paraxial beams in parabolic rotational coordinates.

We point out that one can readily deduce from Eq. (2) that the nonparaxial beams in parabolic rotational coordinates are scalable. In our experiment, the nonparaxial beams in parabolic rotational coordinates are realized by employing the technique of computer-generated holography as reported in our previous work [24,25]. Intensities in Figs. 1–4 have been rescaled for better visualizations. All the normalized intensity is the raw intensity divided by the maximum intensity for simulation; the rescaled intensity is obtained by adjusting the attenuator for the experiment.

Figure 1 shows examples of exact solutions of (00)-, (11)-, and (23)-mode nonparaxial beams from the Helmholtz equation in parabolic rotational coordinates. The side-view propagation [Figs. 1(c), 1(f), 1(i)] and the iso-intensity contour [Figs. 1(j)–1(l)] indicate that the evolution of the beam envelope follows parabolic curves. Figure 1(c) shows that the (00)-mode beam reaches a minimum beam width at  $z = z_0 = 2$  cm, while its axial intensity along the propagation axis alternates between bright and dark distributions, forming bottle-like structures potentially useful for optical trapping [24]. Figures 1(d)–1(f) and 1(g)–1(i), along with the 3D iso-intensity contours [Figs. 1(k) and 1(l)] present examples of high-order mode solutions, where it can be seen that the axial intensity is always minimum (forming a central dark core) due to existence of nonzero vortices (corresponding to  $m = 1$  and  $m = 2$ , respectively).

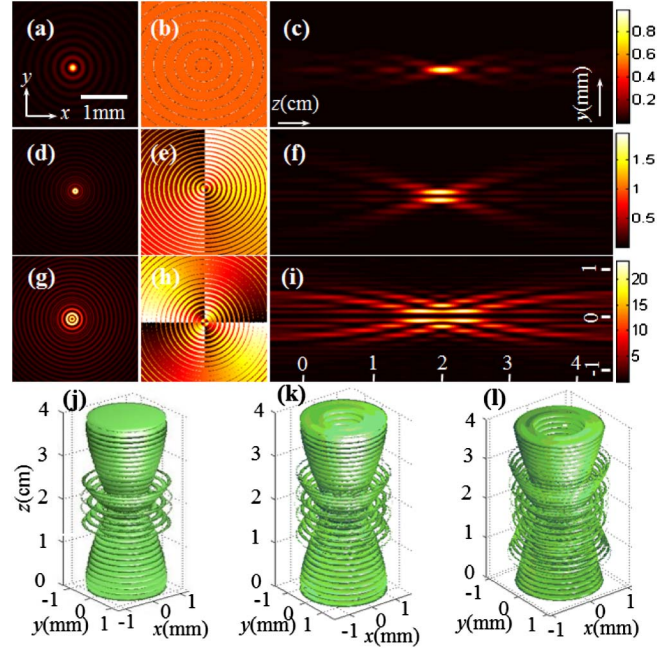


Fig. 1. (a)–(c) Exact (00)-mode; (d)–(f) exact (11)-mode; and (g)–(i) exact (23)-mode nonparaxial beams in parabolic rotational coordinates; (a), (d), (g) normalized amplitude distribution at  $z = 2$  cm; (b), (e), (h) phase distribution at  $z = 2$  cm; (c), (f), and (i) the normalized intensity evolution on the  $x = 0$  plane; iso-intensity contour of (j) exact (00)-mode, (k) (11)-mode, and (l) (23)-mode of the nonparaxial beams in parabolic rotational coordinates;  $z_0 = 2$  cm and  $w_0 = 1$  mm.

Numerical beam propagation and experimental results corresponding to the three modes shown in Fig. 1 are presented in Figs. 2–4. For experimental generation, we launch a broad beam ( $\lambda = 488$  nm) to reconstruct the off-axis holograms of the desired beam profiles encoded in a spatial light modulator [24,25]. The holograms are obtained by computing the off-axis interference

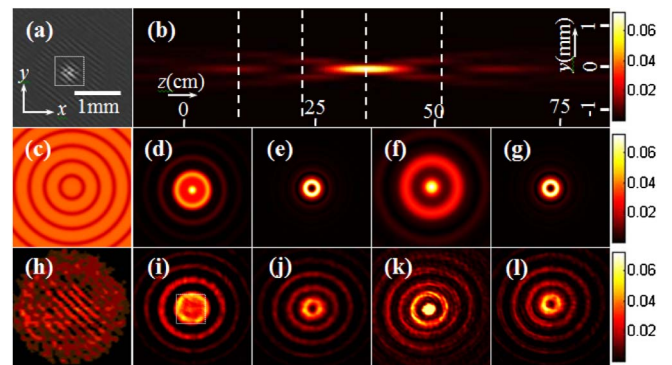


Fig. 2. Numerical and experimental demonstrations of the exact (00)-mode nonparaxial beams in parabolic rotational coordinates. (a) Computer-generated hologram; (b) numerically simulated side-view propagation of the generated beam; (c) phase of the initial generated beam; (d)–(g) snapshots of the normalized transverse intensity patterns taken at the planes marked by the dashed lines in (b); (h) interference phase of the initial generated beam and a plane wave; (i)–(l) experimentally recorded normalized transverse beam patterns at different positions (marked in dashed curve with  $z = 11.7, 24.5, 37.5,$  and  $51$  cm) corresponding to (b);  $z_0 = 37.5$  cm.

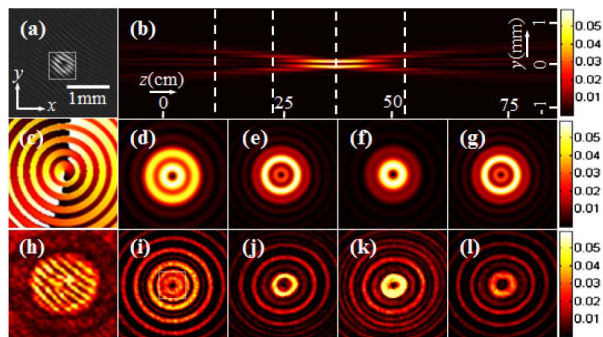


Fig. 3. Description is the same as that in Fig. 2 except the nonparaxial beams in parabolic rotational coordinates are the (11)-mode.

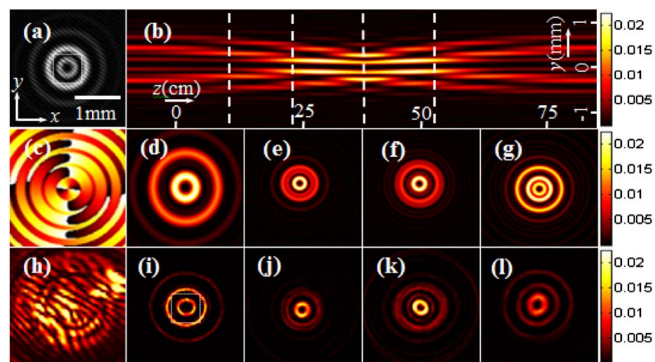


Fig. 4. Description is the same as that in Fig. 2 except the nonparaxial beams in parabolic rotational coordinates are the exact (23)-mode.

patterns between the complex amplitude profile of the parabolic rotational coordinate beams at the  $z = 0$  plane and a plane wave [see Figs. 2(a), 3(a), and 4(a)]. After reflecting from the hologram, the encoded complex amplitude information is rebuilt via a spatial filtering  $4f$  system. The transverse beam patterns at different propagation distances are recorded by a CCD camera, as shown in the bottom panels in Figs. 2–4 for the three different modes. Apparently, the evolution of the rebuilt beam envelope from the hologram follows parabolic curves as shown in Figs. 2(b), 3(b), and 4(b). The transverse intensity patterns taken at different propagation distances indicate clearly that the (00)-mode beam undergoes periodic oscillation in central intensity, varying between bright and dark central spots, whereas the (11)-mode and (23)-mode beams always have dark vortex cores in their axial intensity. Clearly, the nonparaxial beams in parabolic rotational coordinates reach to a minimum beam spot after a certain propagation distance and expand thereafter. These observations are in good agreement with theoretical predictions and numerical simulations.

In summary, 3D nonparaxial beams of parabolic rotational coordinates have been found theoretically by solving the Helmholtz equation and demonstrated experimentally by employing computer-generated

holography. Our experimental results agree well with the theoretical analysis.

This research was supported by NSF, AFOSR, the National Natural Science Foundation of China (11374108, 11304187, 10904041), the Foundation for the Author of Guangdong Province Excellent Doctoral Dissertation (SYBZZXM201227), and the Foundation of Cultivating Outstanding Young Scholars (“Thousand, Hundred, Ten” Program) of Guangdong Province in China.

## References

- W. L. Barnes, A. Dereux, and T. W. Ebbesen, *Nature* **424**, 824 (2003).
- T. W. Ebbesen, H. J. Lezec, H. F. Ghaemi, T. Thio, and P. Wolff, *Nature* **391**, 667 (1998).
- S. A. Maier, P. G. Kik, H. A. Atwater, S. Meltzer, E. Harel, B. E. Koel, and A. A. G. Requicha, *Nat. Mater.* **2**, 229 (2003).
- M. Lax, W. H. Louisell, and W. B. McKnight, *Phys. Rev. A* **11**, 1365 (1975).
- A. Ciattoni, B. Crosignani, and P. Di Porto, *Opt. Commun.* **177**, 9 (2000).
- Q. Cao and X. Deng, *J. Opt. Soc. Am. A* **15**, 1144 (1998).
- G. A. Deschamps, *Electron. Lett.* **7**, 684 (1971).
- G. Rodríguez-Morales and S. Chavez-Cerda, *Opt. Lett.* **29**, 430 (2004).
- Z. Ulanowski and I. K. Ludlow, *Opt. Lett.* **25**, 1792 (2000).
- J. Lekner and R. Boyack, *Opt. Lett.* **35**, 3652 (2010).
- A. April, *J. Opt. Soc. Am. A*, **28**, 2100 (2011).
- A. April, *Opt. Lett.* **33**, 1392 (2008).
- M. A. Alonso, R. Borghi, and M. Santarsiero, *Opt. Express* **14**, 6894 (2006).
- G. A. Siviloglou, J. Broky, A. Dogariu, and D. N. Christodoulides, *Phys. Rev. Lett.* **99**, 213901 (2007).
- Y. Hu, G. Siviloglou, P. Zhang, N. Efremidis, D. Christodoulides, and Z. Chen, in *Nonlinear Photonics and Novel Optical Phenomena*, Z. Chen and R. Morandotti, eds. (Springer, 2012), Vol. **170**, pp. 1–46.
- I. Kaminer, R. Bekenstein, J. Nemirovsky, and M. Segev, *Phys. Rev. Lett.* **108**, 163901 (2012).
- F. Courvoisier, A. Mathis, L. Froehly, R. Giust, L. Furfaro, P. A. Lacourt, M. Jacquot, and J. M. Dudley, *Opt. Lett.* **37**, 1736 (2012).
- P. Zhang, Y. Hu, D. Cannan, A. Salandrino, T. Li, R. Morandotti, X. Zhang, and Z. Chen, *Opt. Lett.* **37**, 2820 (2012).
- P. Zhang, Y. Hu, T. Li, D. Cannan, X. Yin, R. Morandotti, Z. Chen, and X. Zhang, *Phys. Rev. Lett.* **109**, 193901 (2012).
- P. Aleahmad, M.-A. Miri, M. S. Mills, I. Kaminer, M. Segev, and D. N. Christodoulides, *Phys. Rev. Lett.* **109**, 203902 (2012).
- L. C. Lew Yan Voon and M. Willatzen, *Math. Comput. Simul.* **65**, 337 (2004).
- M. Willatzen and L. C. Lew Yan Voon, *Separable Boundary-Value Problems in Physics* (Wiley, 2011).
- M. Abramowitz and I. A. Stegun, *Handbook of Mathematical Functions* (Dover, 1972).
- P. Zhang, Z. Zhang, J. Prakash, S. Huang, D. Hernandez, M. Salazar, D. N. Christodoulides, and Z. Chen, *Opt. Lett.* **36**, 1491 (2011).
- P. Zhang, J. Prakash, Z. Zhang, M. S. Mills, N. K. Efremidis, D. N. Christodoulides, and Z. Chen, *Opt. Lett.* **36**, 2883 (2011).